

O. MOMTAHAN
G.H. CADENA
A. MAKHMALBAF
A. ADIBI[✉]

Two-center holographic recording in highly doped LiNbO₃ crystals

School of Electrical and Computer Engineering, Georgia Institute of Technology,
Atlanta, GA 30332-0250, USA

Received: 8 August 2007/Revised version: 26 September 2007
Published online: 5 February 2008 • © Springer-Verlag 2008

ABSTRACT In this paper, we report the observation of electron tunneling during two-center recording in LiNbO₃:Fe:Mn doped with high Fe concentration. Unlike tunneling in the singly doped lithium niobate that erases the hologram, the effect in two-center recording can improve the diffraction efficiency of the hologram after the recording while it is kept in the dark. A detailed study of this effect in LiNbO₃:Fe:Mn is presented both theoretically and experimentally. We show that the hologram strength may increase or decrease due to tunneling, depending on the experimental condition of recording.

PACS 42.40.-i; 42.70.Ln; 42.40.Lx

1 Introduction

Photorefractive crystals such as lithium niobate (LiNbO₃) have been extensively investigated as holographic recording media [1, 2]. The two-center recording scheme, proposed recently, provides persistent holographic recording in doubly doped lithium niobate [3]. Different efforts on the improvement and optimization of the performance metrics of two-center holographic recording have been reported in the literature for LiNbO₃:Fe:Mn [4–6]. For example, it has been shown that increasing the Fe concentration will result in an increase in the diffraction efficiency. This result is similar to what had been reported before for singly doped LiNbO₃:Fe crystals [2]. However, the maximum concentration for Fe is limited in LiNbO₃:Fe crystals since a hologram recorded in a highly doped crystal will be erased (even in the dark) because of electron tunneling between adjacent Fe sites [7]. We have recently reported that, in theory, high Fe concentrations in a doubly doped crystal used for two-center recording would not necessarily result in the erasure of the stored hologram [6]. In two-center recording, the hologram is eventually stored in the deeper traps (for example, Mn traps in a LiNbO₃:Fe:Mn crystal). Thus, the electron tunneling between the Fe traps will not affect the final hologram that is stored in the Mn traps. Furthermore, the tunneling between the Fe traps during recording

and at the beginning of the readout may result in an increase of the diffraction efficiency of the hologram [6].

It is known that in LiNbO₃:Fe crystals, the tunneling effect is observed for Fe concentrations above 0.05 wt. % Fe₂O₃ [7]. Also, the tunneling effect is observed in LiNbO₃ doped with Mn for doping levels of more than 0.5 wt. % MnCO₃ [8]. The tunneling effect in LiNbO₃:Mn occurs at higher dopant concentrations compared to that in LiNbO₃:Fe since Mn is a deeper trap than Fe. To the best of our knowledge, there is no report on the observation of the electron tunneling in doubly doped LiNbO₃.

In this paper, we present the first experimental evidence for the role of tunneling in two-center recording LiNbO₃:Fe:Mn at high Fe concentrations. We show that at high Fe concentrations, the hologram can even become stronger in the dark due to electron tunneling. We will also show that the effect of tunneling on the two-center recording performance depends strongly on the recording wavelength. In Sect. 2 we explain the experimental configurations and results of recording in LiNbO₃:Fe:Mn with a high Fe concentration. The governing theoretical modeling and analysis are presented in Sect. 3. In Sect. 4 we discuss the effect of tunneling in two-center recording using the experimental and simulation results. Final conclusions are made in Sect. 5.

2 Experimental investigation of electron tunneling in two-center recording

To investigate the evidence of tunneling in two-center recording, a congruently grown LiNbO₃:Fe:Mn crystal with 0.15 wt. % Fe₂O₃ and 0.02 wt. % MnO (grown by Deltronics Crystals) was used. The Fe concentration in this crystal is considerably more than the threshold concentration for electron tunneling in LiNbO₃:Fe. Since the hologram is eventually stored in the Mn traps, the Mn concentration is selected to be lower than the concentration needed for observing electron tunneling between the Mn traps in a LiNbO₃:Mn crystal. Noting the small Mn concentration and the considerably large Fe concentration, we expect to observe the tunneling effect in two-center holographic recording in this crystal. An *x*-cut sample with the size of 10 mm × 10 mm × 2 mm was used in which the *c*-axis lies in the larger face and is parallel to one of the edges. Initially,

✉ Fax: +1-404-894-4641, E-mail: adibi@ece.gatech.edu

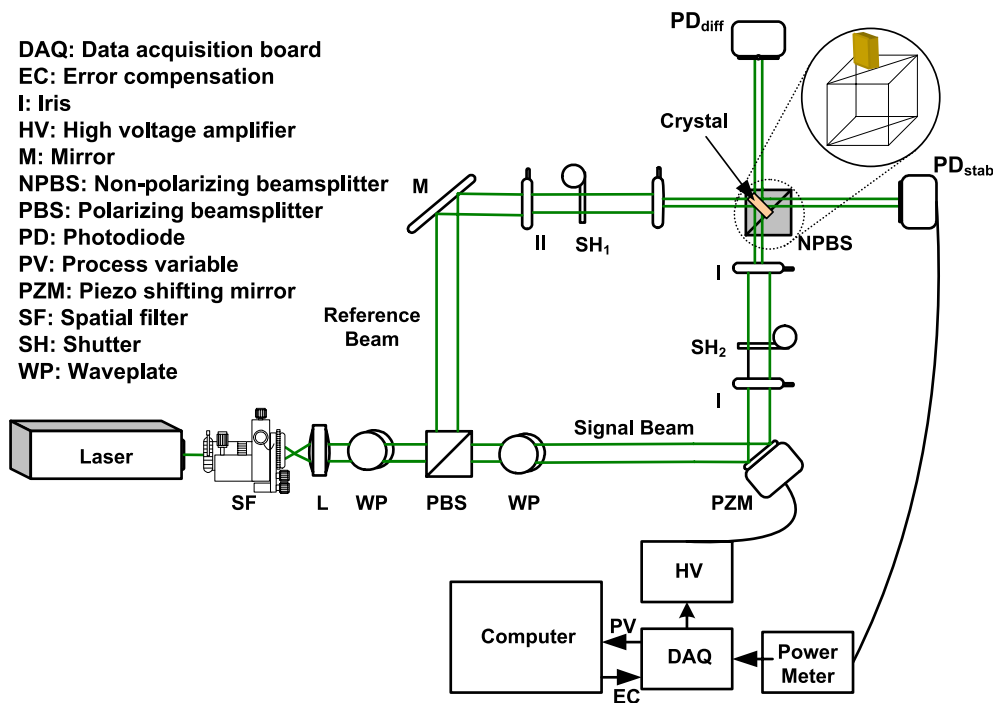


FIGURE 1 The holographic recording setup based on software-based stabilized recording. The movement of the interference pattern is interpreted as a voltage and is sent through a DAQ card into a computer as a process variable (PV) which is then processed in software and returned as an error-compensation (EC) value through a DAQ card to the PZM through a high voltage amplifier. Note that the holographic recording material (shown by the crystal) is mounted on top of the non-polarizing beam splitter (NPBS)

the sample was oxidized in an oxygen atmosphere at 1070 °C for 48 h.

The sample was used in the software-based stabilized recording system shown in Fig. 1 [9]. Two coherent beams (reference and signal beams) at the wavelength of 532 nm or 633 nm (depending on the experiment) and with equal intensities were used to record the holograms in the symmetric transmission geometry. A beam at the wavelength of 404 nm from a cw diode laser was used as the sensitizing beam. In the stabilizer part of the setup, the movement of the interference pattern is interpreted as a voltage and is sent through a data acquisition card (DAQ) to a computer as a process variable (PV). The PV is then processed in software and returned as an error-compensation (EC) value through a DAQ card to the piezo mirror-shifter (PZM) after being amplified through a high voltage amplifier. The diffraction efficiency of the hologram is defined as the ratio of the diffracted beam intensity to the reading beam intensity and was measured using one of the recording beams (i.e., the reference beam). The polarization of the recording beams was TE (i.e. electric field perpendicular to the plane of incidence). The angle of incidence of the reference and signal beams (measure from the normal to the crystal interface) is equal to 45° measured in air.

In the first experiment, a hologram was recorded using two coherent green beams ($\lambda = 532$ nm) and one blue sensitizing beam ($\lambda = 404$ nm) for 30 min. Total recording intensity (i.e., the sum of the intensities of the two recording beams) and the sensitizing intensity were 23 mW/cm² and 10 mW/cm², respectively. Before the recording phase, the hologram was sensitized with the sensitizing beam for 1 hour. After recording, the hologram was illuminated by a Bragg mismatched beam at 532 nm with an intensity equal to the intensity of each of the recording beams (i.e., 11.5 mW/cm²). The readout process started immediately after the recording. The diffraction efficiency of the hologram during the recording and the read-

out was monitored every 60 s by blocking all the beams and using only the reference beam for a short time (1.5 s). The measured diffraction efficiency as a function of time is shown in Fig. 2. As seen in this figure, the dynamic of the recording phase is similar to the conventional two-center recording [4]. However, the readout portion of the curve shows a new behavior not observed before. The diffraction efficiency does not decrease (corresponding to the partial erasure of the hologram [3]) at the beginning of the readout while it is under

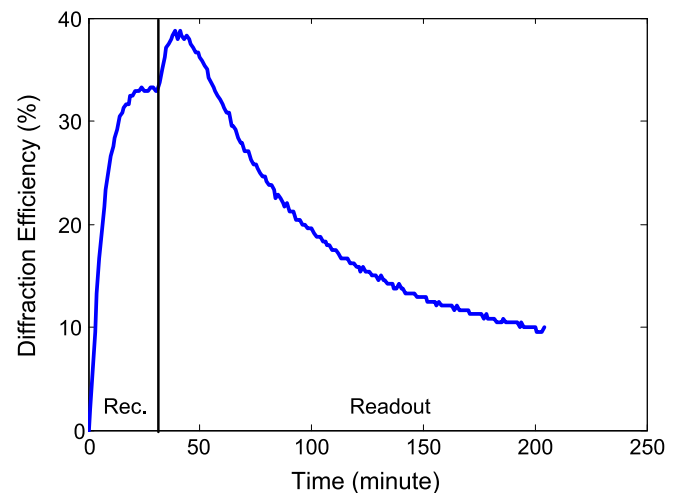


FIGURE 2 Recording-readout curve for a 2 mm thick congruently grown *x*-cut LiNbO₃:Fe:Mn crystal doped with 0.15 wt. % Fe₂O₃ and 0.02 wt. % MnO. The sensitizing and recording wavelengths were 404 nm and 532 nm, respectively. Sensitizing intensity and the total recording intensity were 10 mW/cm² and 23 mW/cm², respectively. The polarization of the recording beams was ordinary. Readout was performed while the crystal was illuminated using a Bragg mismatched green ($\lambda = 532$ nm) beam with an intensity of 11.5 mW/cm². The total angle between the recording beams outside the crystal was 90° in symmetric transmission geometry. Recording time was 30 min

the illumination of the Bragg-mismatched beam. Instead, the diffraction efficiency increases first and then decreases. To reduce the possible experimental uncertainty, the experiment was repeated several times and the same behavior was observed in all the attempts. Note that the hologram was under the illumination of a Bragg mismatched beam during the readout phase and the Bragg-matched reference beam was only used every 60 s for a period of 1.5 s. Therefore, the effect of the reading beam on the hologram is minimal and the increase in the diffraction efficiency during the readout is not due to the two-wave coupling, which is responsible for self-enhancement of the diffraction efficiency during the Bragg-matched readout observed before [10].

To investigate the reason for the increase in the diffraction efficiency after recording, the same experiment was repeated except that after the recording for 30 min, the hologram was kept in the dark for 140 min. The diffraction efficiency of the hologram was monitored in the dark every 60 s by illuminating the hologram with the reference beam with the intensity of 11.5 mW/cm² for 1.5 s. Thus, the total light exposure on the crystal was kept very small to minimize the possible effects on the hologram. After reading in the dark, the hologram was read for another 140 min in the presence of a Bragg-mismatched beam, similar to the one used in the previous experiment, to observe the partial erasure of the hologram. Figure 3 shows the experimental results for this case. As seen in Fig. 3, the diffraction efficiency of the hologram keeps increasing after the recording while being in the dark without any external excitation. To the best of our knowledge, this is the first observation of enhancement of the diffraction efficiency of a hologram recorded in LiNbO₃ crystals without the presence of any illumination or heating. As explained in the following, this effect is a clear indication of electron tunneling in the LiNbO₃:Fe:Mn crystal used in the experiments.

To investigate the effect of the recording conditions on the electron tunneling, we performed a similar experiment using

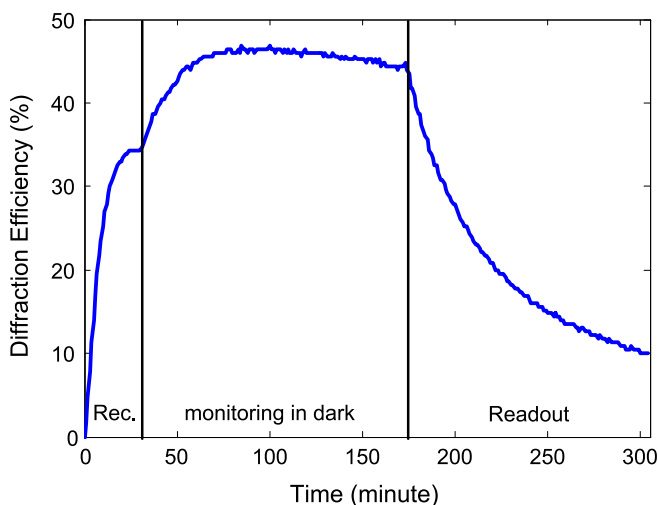


FIGURE 3 Dynamics of the diffraction efficiency for recording, dark monitoring, and readout with exactly the same experimental conditions as those of Fig. 2. After the recording phase the crystal was kept in the dark while the diffraction efficiency of the hologram was monitored every 60 s by illuminating the hologram with the reference beam with the intensity of 11.5 mW/cm² for 1.5 s

two coherent recording beams at the wavelength of 633 nm and a blue sensitizing beam ($\lambda = 404$ nm). The experimental setup is the same as that in Fig. 1 with the laser and the half wave plates (WP's) replaced with the ones operating at $\lambda = 633$ nm. In the recording/readout experiment, the hologram was first recorded for 30 min using two equally intense red beams with a total recording intensity of 200 mW/cm² and a sensitizing beam with an intensity of 18 mW/cm². Immediately after the recording, the intensity of the reference beam was reduced to 5.1 mW/cm². The diffraction efficiency was then monitored every 2 min for 140 min using the low intensity (5.1 mW/cm²) reference beam when the crystal was kept in the dark. The illumination of the hologram with the low intensity beam was limited to 1.5 s for every 2 min to minimize the effect of monitoring on the diffraction efficiency. The variation of the diffraction efficiency of the hologram as a function of time is shown in Fig. 4. It is clear from Fig. 4 that the diffraction efficiency decreases in the dark without any considerable external excitation. This effect is similar to the dark erasure because of the tunneling effect observed in singly doped LiNbO₃:Fe crystals [7]. We believe that the dark erasure shown in Fig. 4 is also due to the electron tunneling in the Fe traps. However, the tunneling effect observed for recording the hologram in the doubly doped crystal using the red beams ($\lambda = 633$ nm) is totally different from that observed for recording using the green beams ($\lambda = 532$ nm), for which the diffraction efficiency increases in the dark. We repeated the experiments for several sets of recording and sensitizing intensities at both wavelengths and obtained similar results consistently. In all the experiments using the green recording beams, after recording the hologram, the diffraction efficiency was either enhanced or remained unchanged in the dark. For recording with the red beams, we always observed the erasure of the hologram in the dark.

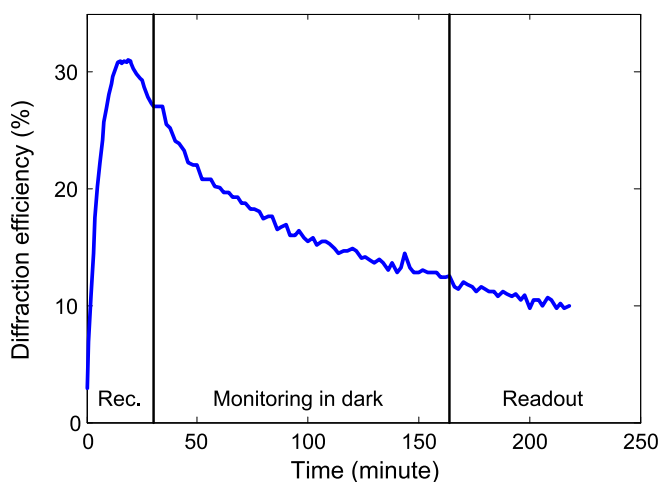


FIGURE 4 Dynamics of the diffraction efficiency for recording, dark monitoring, and readout for a two-center hologram recorded using two red beams. The sensitizing and recording wavelengths were 404 nm and 633 nm, respectively. Sensitizing intensity and the total recording intensity were 18 mW/cm² and 200 mW/cm², respectively. After recording, the hologram was kept in the dark for 140 min and the diffraction efficiency was measured every 2 min by illuminating with the reference beam with the intensity of 5.1 mW/cm² for 1.5 s. During the final readout phase, the hologram was under the illumination of a Bragg-mismatched beam with the intensity of 100 mW/cm². All the other parameters were the same as those in the captions of Fig. 2

3 Modeling the electron tunneling effect in two-center recording

The electron tunneling between the dopant sites in holographic recording in LiNbO_3 crystals is a complicated process. Previous reports provide only the experimental evidences of the tunneling in $\text{LiNbO}_3:\text{Fe}$ and $\text{LiNbO}_3:\text{Mn}$ [7, 8]. Because of the difficulty of the analysis of the electron tunneling during the holographic recording, no complete model is available in the literature. For the electron tunneling in $\text{LiNbO}_3:\text{Fe}$, it is relatively easy to understand the physics of the process. The electrons tunnel between the Fe sites and, thus, redistribute themselves uniformly. The hologram is gradually erased in this process until it is completely vanished when the electrons are uniformly distributed. The tunneling process in two-center recording is more complicated because of the existence of two types of traps (e.g., Fe and Mn in $\text{LiNbO}_3:\text{Fe}:\text{Mn}$). Thus, we need to develop a model to explain the tunneling process in two-center recording.

Because of the large concentration of Fe in the $\text{LiNbO}_3:\text{Fe}:\text{Mn}$ crystal (0.15 wt. % Fe_2O_3) used in our experiments, the average distance between the Fe sites in this crystal is about 2.7 nm, which is small enough to have significant probability for electron tunneling. Also, the electron tunneling from the Fe traps to the Mn traps is possible in this crystal. On average, the Fe traps form a three-dimensional grid with an average distance of 2.7 nm in each direction. Therefore, for any empty Mn site, there might be a filled Fe site at an average distance of 2.7 nm or less. The tunneling from the Fe sites to the Mn sites is an indirect tunneling since the energy of the electron is changed during this process. This tunneling requires exchanging energy with the structure using phonons. However, the tunneling from Mn sites to Fe sites is much less probable as the Mn traps are deeper in the band diagram of the crystal compared to the Fe traps and therefore, the potential barrier is larger for electrons trapped in the Mn sites. Thus, we can conclude that the electron tunneling happens only between the Fe sites and also from the Fe sites to the Mn sites. Also, the electron has a probability for tunneling if an adjacent site (the Fe site or the Mn site) is available (i.e., it is not already occupied by another electron).

When the hologram is recorded inside the crystal, a space-charge electric field is built up, which forms an electric potential. This electric potential modifies the electron energy levels and certainly affects the tunneling process. To understand this better, the energy levels of the conduction band (CB), the valence band (VB), and the Fe dopants are shown in Fig. 5a for a typical $\text{LiNbO}_3:\text{Fe}:\text{Mn}$ crystal after recording a typical hologram using two-center recording. The variation of the energy levels is shown in the direction of the grating vector. The grating period (Λ) is calculated for a hologram recorded with two green beams ($\lambda = 532$ nm) using the setup of Fig. 1. The energy level corresponding to the Mn traps has a similar spatial variation as that of the Fe traps and is not shown in the figure for simplicity. On average, electrons tend to occupy the lower energy states. However, as the electrons mostly go to lower energy levels, by tunneling, they change the charge distribution and, thus, modify the space-charge electric field. As a result, the energy levels in the direction of the grating vector are changed.

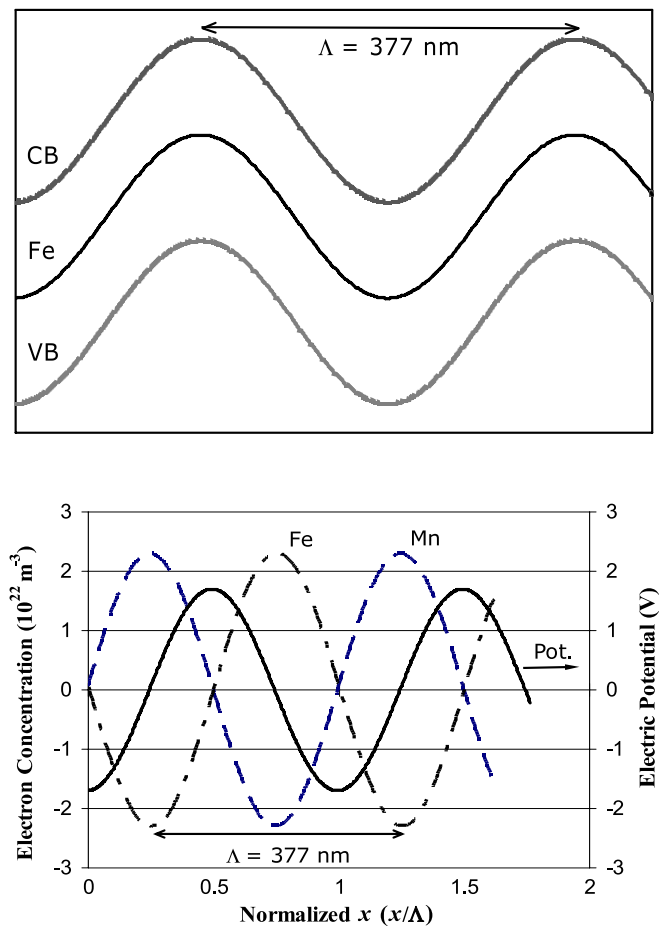


FIGURE 5 (a) The schematic energy levels of the conduction band (CB), the valence band (VB), and the Fe dopants in the presence of the space-charge electric field and (b) the modulated electron concentrations in the Fe and the Mn traps and the built-up electric potential in the direction of the grating vector for a hologram recorded in the $\text{LiNbO}_3:\text{Fe}:\text{Mn}$ crystal. The numerical simulations for the recording were performed based on the two-center model without considering the tunneling effect. All the parameters are the same as those used in the experiment corresponding to Fig. 2. The data is for a hologram recorded for 30 min

Figure 5b shows the modulated electron concentration in the Fe and the Mn traps in the direction of the grating vector in a hologram recorded for 30 min with two plane waves at $\lambda = 532$ nm and with a sensitizing beam at $\lambda = 404$ nm using the setup of Fig. 1. All the parameters are the same as those used in the experiment described in Fig. 2. The numerical simulation for the recording is obtained based on the two-center model [6] without considering the tunneling effect. It is seen in Fig. 5b that the modulated electron concentrations in the Fe and the Mn traps have a phase difference of about 180° (it is actually 179° in Fig. 5b). The electric potential has a phase shift of about -90° with respect to the electron concentration in Fe traps. Therefore, the overall effect of tunneling in the Fe sites is to shift the modulated electron concentration in the Fe traps in a way to occupy the lowest energy states. Also, during this process, the amplitude of the modulated electron concentration in Fe may change since the electrons in regions with higher concentrations tend to go to the regions with lower concentrations (i.e., diffusion of electrons). Considering these two changes in the modulated

electron concentration in the Fe traps, we can simulate the large-scale effect of the electron tunneling as drift-type and diffusion-type currents in the Fe traps only. Note that these are not the actual currents in the conduction band and they are virtually considered between the Fe traps only. Furthermore, we consider the effect of the tunneling from the Fe sites to the Mn sites to be similar to that between the Fe sites but with lower probability since the Mn concentration is about seven times less than the Fe concentration. One major factor that should be considered in both of the tunneling processes is the vacancy of the neighboring states that changes the probability of the tunneling. The average effect of the adjacent vacancy can be considered as a proportional factor that changes the rate of the two components of the tunneling current. For example, for electrons tunneling between the Fe traps, this proportional factor can be simply included in both the tunneling current components by multiplying the rate with the ratio of concentration of the empty Fe sites to the total Fe concentration.

We now modify the model for two-center holographic recording using the assumptions we have made so far to include the effect of tunneling. The tunneling would change the modulated electron concentrations in both traps. The modulated electron concentrations in the traps are very small compared to the average concentrations of electrons in either trap. Thus, we neglect the change in the average electron concentrations in the Mn and the Fe traps during the process.

We assume a sinusoidal variation of the recording intensity, i.e. $I_L = I_{L0}[1 + m \cos(Kx)]$, and consider the first two terms in the spatial Fourier series of all variables, i.e. $N_D = N_{D0} + N_{D1} \exp(-iKx)$. We can find two sets of zeroth and first order equations based on the two-center model as [4, 6]

$$\frac{dN_{D0}^-}{dt} = -(q_{D,L} s_{D,L} I_{L0} + q_{D,H} s_{D,H} I_H) N_{D0}^- + \gamma_D n_0 (N_D - N_{D0}^-), \quad (1)$$

$$\frac{dN_{S0}^-}{dt} = -(q_{S,L} s_{S,L} I_{L0} + q_{S,H} s_{S,H} I_H) N_{S0}^- + \gamma_S n_0 (N_S - N_{S0}^-), \quad (2)$$

$$0 = N_{D0}^- + N_{S0}^- + n_0 - N_A, \quad (3)$$

$$\frac{dN_{D1}^-}{dt} = -(q_{D,L} s_{D,L} I_{L0} + q_{D,H} s_{D,H} I_H) N_{D1}^- - q_{D,L} s_{D,L} m I_{L0} N_{D0}^- + \gamma_D n_1 (N_D - N_{D0}^-) - \gamma_D n_0 N_{D1}^- + \zeta_D N_{S1}^- + \zeta'_D (N_{S1}^- + N_{D1}^-), \quad (4)$$

$$\frac{dN_{S1}^-}{dt} = -(q_{S,L} s_{S,L} I_{L0} + q_{S,H} s_{S,H} I_H) N_{S1}^- - q_{S,L} s_{S,L} m I_{L0} N_{S0}^- + \gamma_S n_1 (N_S - N_{S0}^-) - \gamma_S n_0 N_{S1}^- - \zeta_S N_{S1}^- - \zeta'_S (N_{S1}^- + N_{D1}^-), \quad (5)$$

$$\frac{-iK}{e} j_1 = \left(\frac{dN_{D1}^-}{dt} + \frac{dN_{S1}^-}{dt} + \frac{dn_1}{dt} \right), \quad (6)$$

$$j_1 = e\mu n_0 E_1 - ik_B T \mu K n_1 + (\kappa_{D,L} I_{L0} + \kappa_{D,H} I_H) N_{D1}^- + \kappa_{D,L} m I_{L0} N_{D0}^- + (\kappa_{S,L} I_{L0} + \kappa_{S,H} I_H) N_{S1}^- + \kappa_{S,L} m I_{L0} N_{S0}^-, \quad (7)$$

$$\frac{iK}{e} E_1 = \frac{N_{D1}^- + N_{S1}^- + n_1}{\epsilon \epsilon_0}, \quad (8)$$

where all the parameters are defined in Table 1 with shallower (S) and deeper (D) traps referring to the Fe and the Mn traps, respectively. We have modified (4) and (5) from their original form in two-center recording by adding two terms to each equation corresponding to the electron tunneling effect. For example in (5), the first term added (i.e., $-\zeta_S N_{S1}^-$) represents the redistribution of the electrons in the Fe traps from the regions with higher concentrations to the regions with lower concentrations. This term models the large-scale effect of tunneling as an extra diffusion term in (5). The second term ($-\zeta'_S (N_{S1}^- + N_{D1}^-)$) in (5) represents the redistribution of the electron concentration in the Fe traps by the means of electron tunneling in the presence of an electrical potential. This corresponds to the large-scale drift effect of the tunneling in the presence of the electric field. The space-charge electric field is proportional to the summation of the electron concentrations in the two traps (8). Therefore, the electric potential is also proportional to the total electron concentration as represented in (8). The proper sign is considered to model the motion of the electrons to a lower energy states. The constants ζ_S and ζ'_S are proportional to the tunneling probability of electrons in the Fe traps. For the crystals with lower Fe concentrations, the probability of tunneling is negligible, and therefore, these constants are practically zero. Also, these constants can be functions of the recording parameters. For example, the effect of the existence of vacant neighboring sites for tunneling can be considered as a proportional factor of $(1 - N_{S0}^-/N_S)$ in ζ_S and ζ'_S , where N_S is the total Fe concentration.

The two terms added to (4) are similar to those added to (5) and they represent the diffusion and the drift effects of the electron tunneling from the Fe traps to the Mn traps. Differ-

Notation	Description
$q_{X,Y} s_{X,Y}$	Absorption cross section for absorbing a photon of beam Y and exciting an electron from trap X
$\kappa_{X,Y} s_{X,Y}$	Bulk photovoltaic coefficient of trap X at the wavelength of beam Y
$N_{X,l}^-$	Concentration of ionized dopant X
N_X	Total concentration of a dopant X
N_A	Concentration of positive compensator charge
n_l	Electron concentration
I_Y	Total intensity of beam Y
e	Electron charge
j_l	Current density
k_B	Boltzmann constant
γ_X	Recombination rate of the electrons to trap X
ζ_X	Tunneling parameter corresponding to diffusion effect in trap X
ζ'_X	Tunneling parameter corresponding to drift effect in trap X
K	Magnitude of grating vector
μ	Electron mobility in the conduction band
m	Modulation depth
T	Crystal temperature
t	Time
$\epsilon \epsilon_0$	Permittivity of the crystal

Note l is an integer and can be 1 referring to the first order terms and 0 referring to the zeroth order terms.

X, Y are variables and can get different indices as following:

$X = S$ – Shallower traps

$X = D$ – Deeper traps

$Y = L$ – Lower frequency (longer wavelength) beam

$Y = H$ – Higher frequency (shorter wavelength) beam

TABLE 1 Description of the parameters used in the theoretical modeling

ent constants (ζ_D and ζ'_D) are used for these terms since the probability of tunneling from the Fe sites to the Mn sites is lower than that for tunneling between the Fe sites. Also, the sign of the terms are different from those in (5), since the electrons that are taken from the Fe traps are added to the Mn traps in the process. We assume the relation between the tunneling constants for the two traps to be

$$\zeta_D = \frac{(N_D - N_{D0}^-)}{(N_S - N_{S0}^-)} \zeta_S, \quad (9)$$

$$\zeta'_D = \frac{(N_D - N_{D0}^-)}{(N_S - N_{S0}^-)} \zeta'_S, \quad (10)$$

where N_D is the total Mn concentration. In (9) and (10) we simply assume the probability of tunneling is proportional to the concentration of the vacant neighboring sites as mentioned before. We also assume the variation of the electron concentration in the conduction band (n) is instantaneous compared to the variation of the other variables (adiabatic approximation) [4]. We also assume that the electron concentration in the conduction band is negligible compared to the electron concentrations in the Fe and the Mn traps. These assumptions are all valid for the properties of the crystal and the recording geometry used in our experiments.

4 Simulation results and discussion

In this section, we use the modified two-center recording model explained in Sect. 3 to simulate the experiments presented in Sect. 2. We have developed a model with reasonable assumptions that can explain different phenomena we observed in the experiments. However, the exact simulation of the results presented in Figs. 3 and 4 is not pursued here. Instead, our main purpose here is to show that based on the model, we can expect different recording dynamics by only changing the parameters corresponding to the tunneling in the system of differential equations. Also, as explained before, for low Fe concentrations the tunneling parameters are zero and the model represents the original two-center holographic recording.

We solve the system of differential equations (1)–(8) numerically using Mathematica with the initial conditions of $N_{D0}^-(t=0) = N_D/2$, $N_{S0}^-(t=0) = 0$, $N_{D1}^-(t=0) = 0$, and $N_{S1}^-(t=0) = 0$. After solving for E_1 , the change in the index of refraction through the electro-optic effect and the resulting diffraction efficiency are calculated as explained in [4]. Half of the Mn traps are assumed to be filled with electrons at the beginning of the recording while all the Fe traps are empty. The exact value of the initial electron concentration in the Mn traps is very hard to calculate in this crystal because of the tunneling effect. We used the experimental method introduced in [4] to measure the initial electron concentration in our crystal but the presence of the tunneling effect made the result inconclusive. Instead, we performed several numerical simulations with different values assumed for the initial electron concentrations and the tunneling parameters. The recording dynamics had the best match with the experimental results when 50% of Mn traps are assumed to be initially filled with electrons.

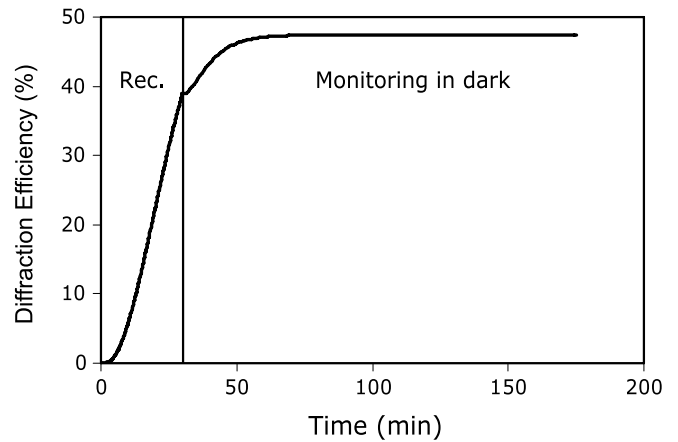


FIGURE 6 Simulation results for the dynamics of the diffraction efficiency during recording and monitoring in the dark when the hologram is recorded using two green beams and a sensitizing blue beam. The model used in the simulation is explained in the text. All the parameters for the simulation are chosen from experimental parameters used to obtain Fig. 2

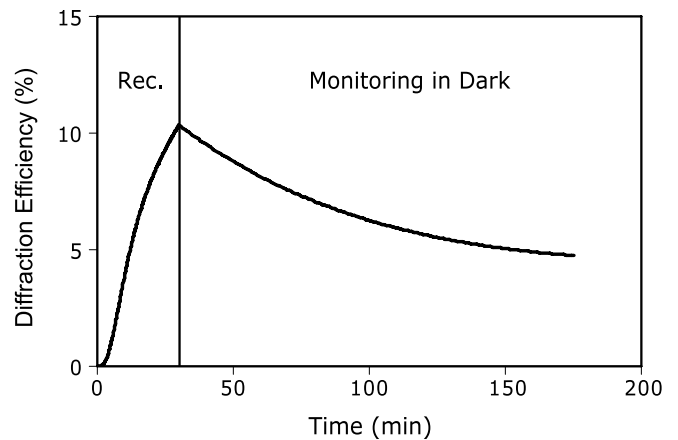


FIGURE 7 Simulation results for the dynamics of the diffraction efficiency during recording and monitoring in the dark when the hologram is recorded using two red beams and a blue sensitizing beam. All the parameters for the simulation are chosen from experimental parameters used to obtain Fig. 4

Figure 6 shows the diffraction efficiency as a function of time obtained by solving the system of equations with all the parameters selected for recording at 532 nm wavelength [4, 6] and are corresponding to the experimental parameters in Fig. 3. The values used for ζ_S and ζ'_S are $2.5 \times 10^{-4} \text{ s}^{-1}$ and $2.1 \times 10^{-3} \text{ s}^{-1}$, respectively, and are obtained by parameter fitting to match the experimental data as explained before. As it is seen in the figure, the diffraction efficiency increases after the recording while the hologram is kept in the dark. This increase is in agreement (qualitatively) with the experimental results observed in Fig. 3.

Figure 7 shows the results when the hologram is recorded using two red beams. All the parameters in the simulation correspond to the experimental condition for the results shown in Fig. 4 and are selected for recording using red beams ($\lambda = 633 \text{ nm}$) [4, 6]. In this case the diffraction efficiency of the hologram is reduced after the recording when it is kept in the dark. For this simulation we obtained and used the values $2 \times 10^{-5} \text{ s}^{-1}$ and $1 \times 10^{-4} \text{ s}^{-1}$ for ζ_S and ζ'_S , respectively, from the parameter fitting. In this case the tunneling effect tends to reduce the diffraction efficiency after the recording.

In two-center recording, the space-charge field is a function of electron concentrations in Mn and Fe traps and the relative phase shift between them. In recording using the red beams and the green beams, the space-charge field and the average concentration of the vacant neighboring Fe sites are different and so is the probability of electron tunneling. This change results in an increase or a decrease in the diffraction efficiency of the hologram when it is monitored in dark after the recording. The exact change of the tunneling probability for recording at different wavelengths is very complicated and cannot be modeled easily. In the two-center recording, the space-charge field is proportional to the sum of the electron concentrations in the two traps (i.e., $N_{S1}^- + N_{D1}^-$). The tunneling effect mostly redistributes the modulated electron concentration in the Fe traps (N_{S1}^-) as the electrons move to lower energy states (the modulated electron concentration in Mn traps (N_{D1}^-) changes slightly). As N_{S1}^- changes, the total space-charge field and the electric potential change accordingly. The effect of this redistribution process is that the space-charge field and, thus, the diffraction efficiency of the hologram decrease. Also, the electron tunneling tries to reduce the modulated electron concentration in the Fe traps. In a singly doped crystal (LiNbO₃:Fe), this effect results in the reduction of the modulated space-charge and thus, the diffraction efficiency. However, in two-center recording in LiNbO₃:Fe:Mn, this effect will increase the total modulated electron concentration (i.e., $N_{S1}^- + N_{D1}^-$) and, therefore, the diffraction efficiency of the hologram. The two tunneling effects have opposite outcomes on the diffraction efficiency of the hologram in two-center recording. In the simulations for recording with red and green beams, we found out that the phase shifts between the electron concentrations in the Mn and the Fe are different in these two cases. In recording with red beams, the phase shift is closer to 180° compared to that for recording with green beams. Therefore, we believe the first tunneling process is mostly dominant in recording with red beams and the diffraction efficiency reduces as the electrons redistribute to make the phase shift between the electron concentration in Mn and Fe equal to 180°. In recording with green, the phase shift between the electron concentrations in the two traps is farther from 180° compared to that for recording with red beams. As the electron concentration in Fe is redistributed by tunneling to reach the 180° phase shift with respect to that in Mn, the electron tunneling reduces the modulated electron concentration in Fe. As the modulated electron concentration in Fe reduces, a larger space-charge field is built up and, therefore, the energy barriers for electrons increases that stops them from further tunneling. This increase in the space-charge field results in an increase in the diffraction efficiency. It should be noted that we have implicitly considered these effects in the constants ζ_D and ζ'_D in our model. These parameters are different in the two cases by one order of magnitude while they

show these completely different variations of the diffraction efficiency monitored after the recording. The exact relation between these parameters and the actual recording conditions at different wavelengths is the topic of the ongoing research.

5 Conclusion

A two-center holographic recording in highly doped LiNbO₃:Fe:Mn was investigated in detail in this paper and the evidence of electron tunneling in a LiNbO₃:Fe:Mn crystal doped with a high Fe concentration was presented for the first time. We experimentally showed that the electron concentration in LiNbO₃:Fe:Mn can increase the diffraction efficiency even when the hologram is kept in the dark. This effect has not been reported to date, to the best of our knowledge, for any hologram recorded in lithium niobate crystal. Based on the physical phenomena involved in the process, the set of equations for two-center recording was modified to include electron tunneling. In this model, we consider electron tunneling between the Fe sites and from the Fe sites to the Mn sites, while the latter has a smaller probability. The large-scale effect of the tunneling is represented as drift and diffusion terms in the two-center model that mostly modifies the electron distribution in the Fe traps. This effect can result in either an increase in the diffraction efficiency or a decrease depending on the tunneling probabilities, which are complicated functions of recording parameters including the recording wavelengths. While the electron tunneling in one-center recording always causes the dark erasure of the holograms, the effect in two-center recording can either erase or enhance the hologram after the recording without any external illumination. We showed here that two-center recording with green ($\lambda = 532$ nm) and sensitizing with blue ($\lambda = 404$ nm) results in hologram enhancement in the dark after the recording. However, two-center recording with red ($\lambda = 633$ nm) and sensitizing with blue ($\lambda = 404$ nm) shows partial erasure in darkness after recording.

ACKNOWLEDGEMENTS This work was supported by the Air Force Office of Scientific Research under contract FA9550-05-1-0438 (G. Pomrenke).

REFERENCES

- 1 D.L. Staebler, J.J. Amodei, J. Appl. Phys. **43**, 1042 (1972)
- 2 A. Yariv, S.S. Orlov, G.A. Rakuljic, J. Opt. Soc. Am. B **13**, 2513 (1996)
- 3 K. Buse, A. Adibi, D. Psaltis, Nature **393**, 665 (1998)
- 4 A. Adibi, K. Buse, D. Psaltis, J. Opt. Soc. Am. B **18**, 584 (2001)
- 5 Y. Liu, L. Liu, C. Zhou, Opt. Lett. **25**, 551 (2000)
- 6 O. Momtahan, A. Adibi, J. Opt. Soc. Am. B **20**, 449 (2003)
- 7 I. Nee, M. Müller, K. Buse, E. Krätzig, J. Appl. Phys. **88**, 4282 (2000)
- 8 Y. Yang, D. Psaltis, M. Luennemann, D. Berben, U. Hartwig, K. Buse, J. Opt. Soc. Am. B **20**, 1491 (2003)
- 9 G. Cadena, O. Momtahan, A. Adibi, Opt. Eng. **45**, 125 801 (2006)
- 10 D. Liu, L. Liu, Y. Liu, C. Zhou, L. Xu, Appl. Phys. Lett. **77**, 2964 (2000)